

Imposing jump conditions in a least squares sense for solving the Poisson equation to high order of accuracy

Alexandre Noll Marques^a, Jean-Christophe Nave^b, Rodolfo Ruben Rosales^c

^a*Department of Aeronautics and Astronautics, Massachusetts Institute of Technology
Cambridge, MA 02139-4307*

^b*Department of Mathematics and Statistics, McGill University
Montreal, Quebec H3A 2K6, Canada*

^c*Department of Mathematics, Massachusetts Institute of Technology
Cambridge, MA 02139-4307*

Abstract

In this paper we are concerned with solving the Poisson equation when the solution is discontinuous across an interface that is not aligned with the computational grid. The *Correction Function Method* (CFM) was developed to solve the Poisson equation in this context, and achieve high order of accuracy using a compact discretization stencil. A key concept behind the CFM is enforcing the jump conditions in a least squares sense by computing integrals over pieces of the interface. However, these computations are challenging when only an implicit representation of the interface is available (*e.g.*, the zero contour of a level set function), especially in 3-D. In this paper we address this challenge by introducing a new technique for imposing the jump conditions in a least squares sense. This technique depends only on integrals over sections of the interface that are amenable to numerical quadrature after appropriate coordinate transformations. We incorporate this technique into a fourth order accurate implementation of the CFM, and show examples of solutions computed in 2-D and 3-D.

Keywords: Correction Function Method, Embedded interface, Poisson equation, High accuracy, Gradient-Augmented Level Set Method

PACS: 47.11-j, 47.11.Bc

2010 MSC: 76M20, 35N06

1. Introduction

Solving the Poisson equation in the presence of discontinuities is of great importance in many applications of science and engineering. In many cases, the discontinuities are caused by interfaces between different media, such as in multiphase flows, the Stefan problem, Janus drops, and other multiphase phenomena. These interfaces are themselves solutions to differential equations, and can assume complex configurations. For this reason, it is convenient to embed the interface into a regular triangulation or Cartesian grid and solve the Poisson equation in this regular domain. The Correction Function Method (CFM) [1–3] was developed to solve the Poisson equation in this context, and achieve high order of accuracy with a compact discretization stencil.

One of the key concepts behind the CFM is enforcing the jump conditions in a least squares sense. Although this concept is partly responsible for the robustness of the CFM (as explained in §2), it poses a challenge for implementing previous versions of the CFM in 3-D. Namely, the least squares procedure requires evaluating integrals over pieces of the interface, which is especially difficult in 3-D when only an implicit representation of the interface is available (*e.g.*, the zero contour of a level set function). In this paper we address this challenge by introducing a new technique for imposing the jump conditions in a least squares sense. In this technique, the interface is split into small sections that are amenable to numerical quadrature after appropriate coordinate transformations. The jump conditions are then applied to each section individually, and their effects are combined in a least squares sense. This technique can be seamlessly applied in 2-D and 3-D. Moreover, throughout this paper we assume that an explicit representation of the interface is not available.

The general Poisson equation with discontinuous solution is given by

$$\nabla \cdot (\beta(\vec{x}) \nabla u(\vec{x})) = f(\vec{x}) \quad \text{for } \vec{x} \in \Omega, \quad (1a)$$

$$[u(\vec{x})] = a(\vec{x}) \quad \text{for } \vec{x} \in \Gamma, \quad (1b)$$

$$[\beta(\vec{x}) u_n(\vec{x})] = b(\vec{x}) \quad \text{for } \vec{x} \in \Gamma, \quad (1c)$$

$$u(\vec{x}) = g(\vec{x}) \quad \text{for } \vec{x} \in \partial\Omega. \quad (1d)$$

The solution domain Ω is split into two sub-domains, Ω_1 and Ω_2 , by a co-dimension 1 surface, Γ , disjoint from the boundary $\partial\Omega$. This situation is illustrated in figure 1. Furthermore, a and b are known functions defined on

Γ , and the brackets denote the jump in the enclosed quantity across Γ , *e.g.*,

$$[u(\vec{x})] = \lim_{\substack{\vec{x}^* \rightarrow \vec{x} \\ \vec{x}^* \in \Omega_2}} u(\vec{x}^*) - \lim_{\substack{\vec{x}^* \rightarrow \vec{x} \\ \vec{x}^* \in \Omega_1}} u(\vec{x}^*). \quad (2)$$

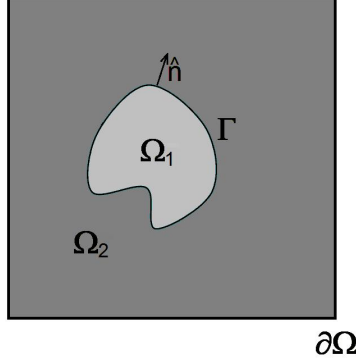


Figure 1: Illustration of the solution domain for the discontinuous Poisson equation. The domain Ω is split into two subdomains, Ω_1 and Ω_2 , by the internal interface Γ .

In general, β is a known positive function that can also be discontinuous across the interface Γ . However, in this paper we only consider the case where β is constant. As mentioned above, the focus of this paper is on how to impose the jump conditions in a least squares sense when only an implicit representation of the interface is available. The case of discontinuous β introduces additional difficulties that are not related to the focus of this paper. We address some of these difficulties in ref. [3] by coupling the CFM with boundary integral equations. However, solving boundary integral equations to high order of accuracy using level set functions is also a challenge. For this reason, we will introduce a more general framework for the case of discontinuous β in a paper that is currently in preparation.

Moreover, in this paper we assume that the boundary $\partial\Omega$ is perfectly aligned with the computational grid, such that the Dirichlet boundary condition in (1d) can be easily replaced by others, such as Neumann, Robin, or mixed. Our concern here is on how to deal with the jump conditions at the interface Γ .

Over the past four decades, several methods have been developed to solve (1), and other closely related problems, with either an interface or a

boundary that is embedded into a regular triangulation or Cartesian grid [4–33]. One of the shortcomings of many embedded methods is that they are restricted to first or second order of accuracy. However, there are exceptions – methods that achieve accuracy higher than second order – and these are based on one of the following ideas: (i) discretization stencils that incorporate the jump (or boundary) conditions [15–17, 22, 23], or (ii) smooth extrapolations of the solution constrained by the jump (or boundary) conditions [13, 27–29]. In practice these ideas are implemented by Taylor expansion or a similar concept, and high order of accuracy is obtained at the expense of wide discretization stencils. In turn, wide stencils may introduce additional issues, such as handling multiple crossings of the interface by a single stencil, and restrictions on the proximity between interfaces. The method introduced by Mayo and collaborators [15–17] avoids wide discretization stencils by incorporating second and third derivatives of the jump conditions into the Taylor expansion. On the other hand, computing higher derivatives of the jump conditions requires the solution of an additional boundary integral equation.

In contrast to using Taylor expansion, the CFM [1–3] is based on computing a smooth extension of the solution by solving a partial differential equation that is compatible with the underlying Poisson problem. This concept results in a general framework that, in principle, can achieve arbitrary order of accuracy, and maintains compact discretization stencils. In ref. [1] we introduce the fundamentals of the CFM, and detail a fourth order implementation to solve (1) in 2-D when β is constant. In ref. [3] we extend the CFM to solve (1) with piece-wise constant β , including the possibility of arbitrarily large jumps in the equation’s coefficients (in [3] we show third order convergence for coefficient ratios of $1 : 10^6$). The work of ref. [3] is inspired by Mayo’s method, and also requires the solution of a boundary integral equation. However, there is an extension of the CFM for the case of discontinuous β that does not require the solution of a boundary integral equation. This extension is briefly discussed in ref. [2], and is the subject of a paper that is in preparation. The CFM has also been extended to other classes of differential equations, such as the heat equation [2], the Navier-Stokes equations [2], and the wave equation [34]. An overview of the CFM for the Poisson equation is presented in §2.

One of the key features of the CFM is the fact that it enforces the jump conditions (1b–c) in a least squares sense. This feature, combined with an

appropriate representation of the solution, is responsible for the robustness¹ of the method with respect to the arbitrary fashion an interface can cross a regular computational grid. However, this feature requires accurate computations of surface integrals over pieces of the interface. These computations are particularly challenging in 3-D when the interface is represented by a level set function defined on a regular grid.

In this paper we present a new technique to impose the jump conditions in a least squares sense. This technique computes integrals only over sections of the interface that are amenable to numerical quadrature, and it is based on the combination of (i) splitting the interface into small sections, (ii) defining local coordinate transformations that map these sections into squares, and (iii) an efficient scheme to compute of the transformations between local and global coordinates. Furthermore, this can be applied to the CFM with only small modifications to the original CFM formulation. The result is a method to solve (1) that achieves high order of accuracy, uses compact discretization stencils, and can be implemented efficiently when the interface is represented by a level set function, both in 2-D and 3-D. The details are discussed in §3.

This paper is organized as follows. In §2 we present an overview of the CFM for the Poisson equation and the features relevant to the new formulation. Next, in §3 we present the details of the new technique for imposing the jump conditions in a least squares sense, including its effects in the CFM formulation. In §4 we present solutions computed with the new formulation of the CFM in 2-D and 3-D. Finally, the conclusions are in §5.

2. Overview of the Correction Function Method

The Correction Function Method (CFM) was developed to solve the Poisson equation (1) when the solution is discontinuous across an interface that is not aligned with a computational grid [1–3]. The CFM offers a general framework to produce discretizations of this problem to high order of accuracy. For instance, in ref. [1] we show a fourth order implementation of the CFM in 2-D for the problem where β is constant. In ref. [3] we show a third order implementation of the CFM, also in 2-D, for the problem where β is piece-wise constant. In this paper we focus on the implementation of

¹By robustness we mean that no special cases need to be considered. Also, the CFM is robust because there are no restrictions on the proximity between interfaces. In §4 we show examples in which interfaces touch each other.

the CFM in 3-D when the interface is represented by a level set function defined on a grid. For the sake of simplicity, we restrict our presentation to the case where β is constant.

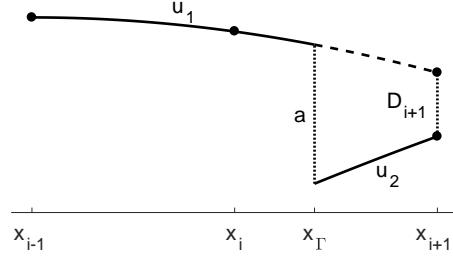


Figure 2: Illustration of the use of the correction function to correct a discretization stencil. D_{i+1} is used to write $u_{1,i+1} = u_{2,i+1} - D_{i+1}$, which can be used to compute u_{xx_i} using (4).

The CFM is based on the notion of smooth extensions of the solution across the interface (denoted by u_1 and u_2), and the definition of the *correction function*: $D = u_2 - u_1$. The correction function can be used to correct a discretization stencil when it crosses the interface. To illustrate this point, consider the approximate computation of u_{xx} at grid node i using standard centered finite differences:

$$u_{xx_i} \approx \frac{u_{i-1} - 2u_i + u_{i+1}}{h^2}, \quad (3)$$

where h is a uniform grid spacing. Equation (3) is known to produce errors $\mathcal{O}(h^2)$ if $u \in C^2((x_{i-1}, x_{i+1}))$. However, when u is discontinuous, as depicted in figure 2, (3) can result in large errors that do not decrease as the computational grid is refined. One way to address this issue, originally introduced in the Ghost Fluid Method [24–26], is to estimate a smooth extension of the solution across the interface before applying the discretization. In practice, only the difference between the smooth extension and the actual grid values are needed. In the case depicted in figure 2, an estimate of $D_{i+1} = u_{2,i+1} - u_{1,i+1}$ can be used to correct (3) as follows:

$$u_{xx_i} \approx \frac{u_{i-1} - 2u_i + u_{i+1}}{h^2} - \frac{D_{i+1}}{h^2}. \quad (4)$$

To achieve high order of accuracy, the correction D needs to be computed to at least the same order as discretization to the underlying Poisson equation.

Some methods use Taylor expansions to estimate D [25, 26] or, equivalently, smooth extrapolations of u [24, 27–29]. In contrast, the CFM computes D by solving a partial differential equation defined on a narrow band of width $\mathcal{O}(h)$ that surrounds the interface. As shown in ref. [1], when β is constant, the correction function is defined as the solution to the following equation,

$$\nabla^2 D(\vec{x}) = (f_2(\vec{x}) - f_1(\vec{x}))/\beta = f_D(\vec{x}) \quad \text{for } \vec{x} \in \Omega_\Gamma, \quad (5a)$$

$$D(\vec{x}) = a(\vec{x}) \quad \text{for } \vec{x} \in \Gamma, \quad (5b)$$

$$D_n(\vec{x}) = b(\vec{x}) \quad \text{for } \vec{x} \in \Gamma, \quad (5c)$$

where Ω_Γ denotes the narrow band around the interface in which the correction function exists.

Remark 1. Equation (5) is an elliptic Cauchy problem. In a continuous setting, this problem is ill-posed because small perturbations to the interface conditions (5b-c) result in arbitrarily large changes in the solution. However, in a numerical setting, where disturbances to (5b-c) are restricted to a finite wave length, it is possible to develop well behaved numerical schemes to solve this problem in a narrow band surrounding the interface. The least squares approach used in the CFM (discussed below) is one such numerical scheme. In ref. [1] we explain the implications of using this method in terms of conditioning. ♣

In practice, it is convenient to solve (5) locally whenever the stencil used to discretize the Laplace operator in (1a) crosses the interface. Namely, (5) is solved in small cubic patches Ω_{Γ_i} , $i \in S_\Gamma$, where S_Γ denotes the set of all grid nodes that are part of a stencil that crosses the interface. These patches are constructed using the “node-centered” approach [1] described next.

The construction of a patch Ω_{Γ_i} is illustrated in figure 3(a). We suggest the reader to refer to this figure while reading the description that follows. Let \vec{x}_i denote the location of the grid node $i \in S_\Gamma$, and let ℓ_d denote a characteristic length of the discretization stencil. Then, the center of the patch Ω_{Γ_i} , denoted by \vec{x}_0 , is defined by an approximate projection of \vec{x}_i onto the interface:

$$\vec{x}_0 = \vec{x}_i - \phi(\vec{x}_i) \left(\frac{\vec{\nabla} \phi(\vec{x}_i)}{|\vec{\nabla} \phi(\vec{x}_i)|^2} \right), \quad (6)$$

where ϕ is the level set function used to represent the interface. Furthermore, the patch is oriented such that the plane tangent to the interface at

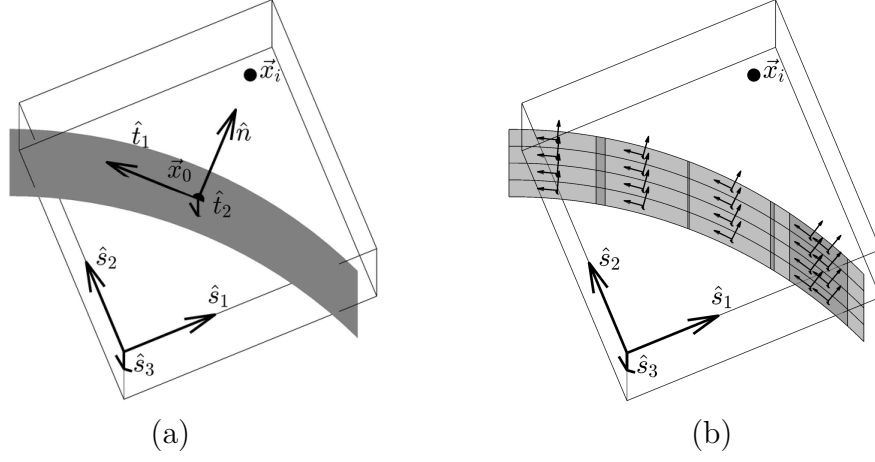


Figure 3: (a) Cubic patch used to define the *correction function* in 3-D. (b) Interface integrals are evaluated over quasi-flat sections of the interface. Sections may overlap, and one patch may contain several sections.

\vec{x}_0 coincides with one of the diagonals of the patch. Algorithm 1 summarizes the computation of \vec{x}_0 , and the triad of unit vectors $\{\hat{s}_d\}_{d=1,2,3}$ that defines the orientation of the patch. Finally, Ω_{Γ_i} is the cubic region of edge length ℓ_d that is centered at \vec{x}_0 and aligned with $\{\hat{s}_d\}$.

The correction function is computed within each patch Ω_{Γ_i} by solving (5) in a least squares sense. This approach makes the solution robust with respect to the arbitrary fashion the interface can cross the computational grid. Specifically, the CFM formulation introduced in ref. [1] is based on solving (5) by minimizing the following functional,

$$\begin{aligned}
 J_i = & \frac{\ell_d^4}{V_i} \int_{\Omega_{\Gamma_i}} (\nabla^2 D - f_D)^2 dV \\
 & + \frac{c_P}{S_i} \int_{\Gamma \cap \Omega_{\Gamma_i}} [(D - a)^2 + \ell_d^2 (D_n - b)^2] dS,
 \end{aligned} \tag{7}$$

where $V_i = \ell_d^3$ is the volume of the patch Ω_{Γ_i} , S_i is the area of the piece of interface contained within the patch, and c_P is a penalization coefficient used to enforce the jump conditions. Note that it is not necessary for the second integral in (7) to be over exactly the intersection of the interface with the patch, which is hard to compute in 3-D. This integral just needs to be over a piece of the interface which is approximately the size of this intersection.

Algorithm 1 Patch for the solution of the correction function around node \vec{x}_i .

- 1: $\phi_i \leftarrow \phi(\vec{x}_i),$
 $\vec{\nabla}\phi_i \leftarrow \vec{\nabla}\phi(\vec{x}_i)$
 - 2: $\vec{x}_0 \leftarrow \vec{x}_i - \phi_i \vec{\nabla}\phi_i / |\vec{\nabla}\phi_i|^2,$
 $\vec{\nabla}\phi_0 \leftarrow \vec{\nabla}\phi(\vec{x}_0)$
 - 3: $\hat{n} \leftarrow \vec{\nabla}\phi_0 / |\vec{\nabla}\phi_0|$
 - 4: $[\hat{t}_1, \hat{t}_2] \leftarrow \text{tangent}(\hat{n})$ ▷ see algorithm 2
 - 5: $\hat{s}_1 \leftarrow (\hat{n} - \hat{t}_1) / \sqrt{2}$
 - 6: $\hat{s}_2 \leftarrow \hat{t}_2 \times \hat{s}_1$
 - 7: $\hat{s}_3 \leftarrow \hat{t}_2$
-

Algorithm 2 Computation of tangent vectors. $[\hat{t}_1, \hat{t}_2] = \text{tangent}(\hat{n})$. This algorithm is based on ref. [26].

- 1: Determine \hat{e}_{\min} such that
 $\hat{n} \cdot \hat{e}_{\min} = \min(n_1, n_2, n_3)$
 - 2: $\hat{t}_1 \leftarrow \hat{n} \times \hat{e}_{\min}$
 - 3: $\hat{t}_2 \leftarrow \hat{n} \times \hat{t}_1$
-

Relaxing this constraint is essential to the technique discussed in §3. In §3 we also discuss how to modify J_i to incorporate the interface integrals computed with the new technique.

The accuracy of the CFM stems from the fact that the correction function is defined as the solution to a PDE, which, in principle, can be solved to arbitrary order of accuracy. In the method described above, the accuracy is determined by the choice of basis functions used to represent D within each patch. In this paper, as in ref. [1], we obtain fourth order of accuracy by representing D with Hermite cubic interpolants.

Once the correction function D is known, it can be used to complete the discretization stencil whenever it straddles the interface, as illustrated by (4). Furthermore, because the correction function depends only on known parameters of the problem – a , b , f , and the position of Γ – the CFM produces modifications to the right-hand-side of the discretized equations only. As a result, one can solve the Poisson equation by inverting the exact same linear system as in problems with no interface, but with a modified right-hand-side.

In addition, note that the PDE that defines correction function, and the least squares procedure used to solve it, do not depend on the computational grid. Hence, the CFM is applied exactly the same way for every discretization stencil that crosses the interface, and no special cases need to be considered. This feature makes the CFM very robust with respect to the arbitrary fashion an interface can cross the computational grid.

On the other hand, the least squares approach introduces the challenge of computing the surface integrals in (7) accurately. In ref. [1] the CFM is implemented only in 2-D, such that the interfaces are 1-D curves. In this context, the level set information (specifically, the Gradient-Augment Level Set Method of [35]) is used to create local parametrizations of these curves within each patch. Once these parametrizations are known, the surface integrals become simple to evaluate. However for 3-D problems, finding surface parametrizations based on level set information is significantly more challenging. In the next section we present an alternative approach to evaluate the surface integrals, which is suitable for implementations in 2-D and in 3-D.

3. Imposing jump conditions in a least squares sense

As discussed in §2, the CFM computes the correction function by solving the PDE (5) locally within several quadrangular patches (Ω_{Γ_i}) that surround

the interface. Within each patch, the CFM solves (5) by minimizing the functional J_i , which corresponds to imposing the PDE and the jump conditions in a least squares sense, see (7). The challenge in this approach is that the surface integrals in J_i can be difficult to evaluate, especially when only an implicit representation of the of the interface is available. This difficulty stems from the fact that the patches can intersect the interface in an arbitrary fashion. Hence, finding a numerical quadrature over $\Gamma \cap \Omega_{\Gamma_i}$ is not trivial. However, it is possible to impose the jump conditions in a least squares sense by using integrals over a slightly different piece of the interface that is more amenable to numerical quadrature. In this section we present a technique that is based on this premise.

Our goal is to impose jump conditions over a piece of the interface that includes enough information to define a unique solution to (5) within each patch Ω_{Γ_i} . In ref. [1] we show that imposing the jump conditions over a piece of the interface that is approximately the size of one of the diagonals of the patch works well in practice. This heuristics is reflected in the construction of the patch Ω_{Γ_i} (see §2), whose orientation is selected to approximately maximize the intersection of the surface with the patch, and in imposing the jump conditions over $\Gamma \cap \Omega_{\Gamma_i}$. However, the jump conditions can be imposed on any piece of the interface that is approximately the size of one of the diagonals.

A convenient choice is to impose the jump conditions over a “quadrangular” piece of the interface, *i.e.*, a piece of the interface that can be mapped into a square by an affine transformation. If the transformation is bijective, one can use a numerical quadrature defined on the square to compute the integrals over the quadrangular piece of the interface. Furthermore, to guarantee that such a bijective transformation always exists, we split the interface into small quasi-flat sections and impose the jump conditions on the union of these sections. Nevertheless, because the interface is represented implicitly, it is not practical to define a transformation that acts on the interface alone. Instead, we introduce a local coordinate transformation that acts on \mathbb{R}^3 which, when restricted to the interface, defines an affine transformation that maps a section of the interface onto a square, even though the coordinate transformation itself may be nonlinear.

Hence, we introduce a technique for imposing jump conditions in a least squares sense that is based on (i) splitting the interface into several quasi-flat quadrangular sections – see figure 3(b), (ii) defining local coordinate transformations that map each of these sections onto a square, and (iii) introducing

an approximate scheme to compute the mapping from the square back onto the interface sections. In §3.1 we introduce the local coordinate transformation, and discuss how to split the interface into small quasi-flat sections over which the transformation is bijective. In §3.2 we present an approximate scheme to compute the inverse transformation, which maps the square back a section of the interface. Finally, in §3.3 we discuss how to modify the functional J_i to impose jump conditions in a least squares sense by evaluating the integrals over quadrangular sections of the interface.

3.1. Local coordinate transformation

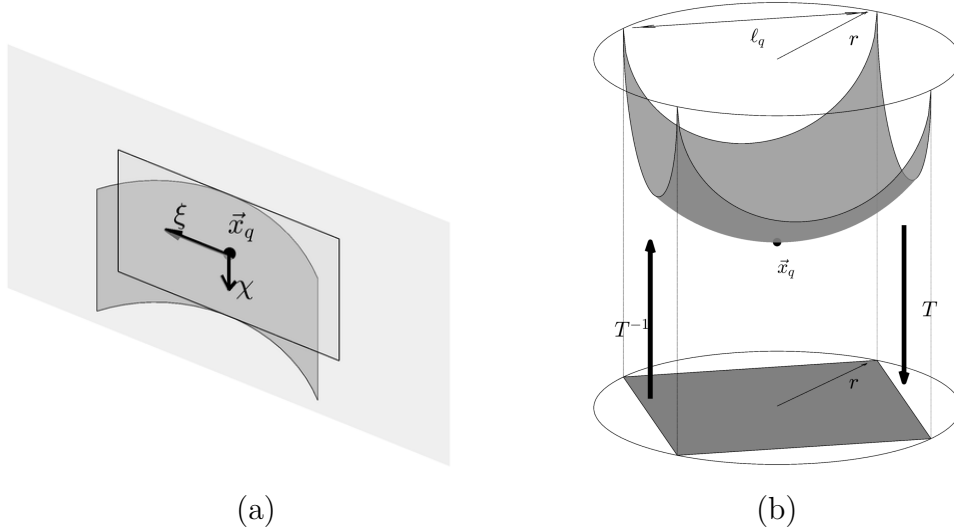


Figure 4: (a) Coordinates ξ and χ are defined by the orthogonal projection onto the plane tangent to the interface at \vec{x}_q . (b) Transformation T on a quadrangular section of the surface of a sphere of constant curvature. The transformation is bijective if $\ell_q < \sqrt{2}r$. For general surfaces, $\ell_q < \sqrt{2}r_{\min}$ is a conservative upper bound on ℓ_q that guarantees that the transformation is bijective.

Let \vec{x}_q denote a point on the interface. We are interested in defining a local coordinate transformation, $T : (x, y, z) \mapsto (\xi, \eta, \chi)$, such that a section of the interface in neighborhood of \vec{x}_q is mapped by T onto a square. To achieve this goal, we first define one of the coordinates as an approximation to the signed distance function: $\eta = \phi / |\vec{\nabla} \phi(\vec{x}_q)|$. As a consequence, the interface lies on the $\eta = 0$ surface. Then, the other coordinates are given by an orthogonal projection onto the plane tangent to the interface at \vec{x}_q , as depicted

in figure 4(a). The computation of the transformation T is summarized in algorithm 3.

Algorithm 3 Transformation T in the neighborhood of \vec{x}_q .

- 1: Determine tangent plane at \vec{x}_q

$$\vec{\nabla}\phi_q \leftarrow \vec{\nabla}\phi(\vec{x}_q)$$

$$\hat{v}_1 \leftarrow \vec{\nabla}\phi_q/|\vec{\nabla}\phi_q| \quad \triangleright \text{normal vector}$$

$$[\hat{v}_2, \hat{v}_3] \leftarrow \text{tangent}(\hat{v}_1) \quad \triangleright \text{tangent vectors, see algorithm 2}$$
 - 2: Define η

$$\bar{\phi} \leftarrow |\vec{\nabla}\phi_q|$$

$$\eta(\vec{x}) = \phi/\bar{\phi}$$
 - 3: Define ξ and χ

$$\xi = \hat{v}_2 \cdot (\vec{x} - \vec{x}_q) \quad \triangleright \text{projection onto tangent plane}$$

$$\chi = \hat{v}_3 \cdot (\vec{x} - \vec{x}_q)$$
-

Furthermore, let $r_{\min} > 0$ denote the minimum radius of curvature of the interface in a neighborhood of \vec{x}_q . Then, as illustrated in figure 4(b), for any $\ell_q < \sqrt{2}r_{\min}$, the inverse transformation T^{-1} exists on the square

$$Q := \{\eta = 0 \text{ and } (\xi, \chi) \in [-\ell_q/2, \ell_q/2]^2\}, \quad (8)$$

and $T^{-1}(Q)$ is a quadrangular piece of the interface centered at \vec{x}_q and with area approximately equal to ℓ_q^2 . In practice, however, we take ℓ_q to be smaller than this upper limit to guarantee accuracy in the computation of the inverse transformation. We discuss the practical limits on ℓ_q in §3.2.

Remark 2. Note that the quadrangular piece of the interface that is mapped onto the square Q is defined implicitly by $T^{-1}(Q)$. One can only choose the “center” of the transformation, \vec{x}_q , and the “length” of the section, ℓ_q . ♣

Note also that \vec{x}_q is not required to lie exactly on the interface. If \vec{x}_q is relatively close to the interface (with respect to ℓ_q), then ξ and χ are given by an orthogonal projection onto a plane that is approximately tangent to the interface, which is enough to define a bijective transformation following algorithm 3.

In our implementation of the present technique, we use the computational grid on which the level set function is represented to locate the centers (\vec{x}_q)

of the local transformations, and to define ℓ_q . Let us denote this grid by G_Γ , with characteristic grid spacing h_Γ . Then, for each cell on G_Γ that crosses the interface, we set \vec{x}_q as the approximate projection of the center of the cell onto the interface:

$$\vec{x}_q = \vec{x}_c - \phi(\vec{x}_c) \left(\frac{\vec{\nabla}\phi(\vec{x}_c)}{|\vec{\nabla}\phi(\vec{x}_c)|^2} \right), \quad (9)$$

where \vec{x}_c denotes the center of the cell. Furthermore, we associate with this cell a quadrangular section of interface of characteristic length $\ell_q = h_\Gamma$. Therefore, we use the grid G_Γ to split the interface into several quasi-flat sections.


Finally, to guarantee that ℓ_q can be always made as small as needed, the grid used to represent the level set function may be distinct from the grid used to solve the Poisson equation. We make this distinction explicit by denoting the grid in which the Poisson equation is solved by G_P , with characteristic grid spacing h_P .

3.2. Inverse transformation

The efficiency of the present technique relies on the fact that the inverse transformation T^{-1} is not computed exactly. Instead, the inverse transformation is approximated using polynomials of the same degree as the level set representation. This approximation is justified because we assume that the interface is locally quasi-flat. This assumption implies that

$$T \circ T_{\text{approx}}^{-1} = I + \mathcal{O}(h_\Gamma^{p+1}),$$

where T_{approx}^{-1} denotes the approximate inverse transformation, and the degree of polynomials used in the level set representation is $3p$ (or $2p$ in 2-D).

Sketch of the proof. Since the interface is quasi-flat, the inverse transformation T^{-1} exists and is smooth in a neighbourhood of the interface. Hence, we can always approximate this inverse transformation with a polynomial. In the case of a polynomial of degree $3p$, we can guarantee that $T_{\text{approx}}^{-1} = T^{-1} + \mathcal{O}(h_\Gamma^{p+1})$. Furthermore, since the forward transformation is composed of polynomials of degree at most $3p$, it is easy to show that $T \circ T_{\text{approx}}^{-1} = I + \mathcal{O}(h_\Gamma^{p+1})$. 

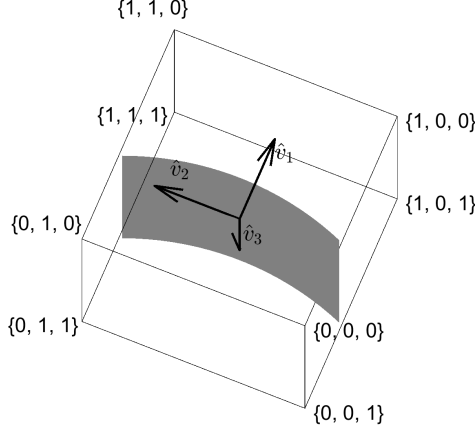


Figure 5: h_{Γ}^3 cube centered on \vec{x}_q and aligned with $\hat{v}_1 - \hat{v}_2 - \hat{v}_3$.

The approximate inverse transformation is computed as follows. Each transformation $T_{\text{approx}}^{-1} : (\xi, \eta, \chi) \mapsto (x, y, z)$ is approximated by three p -th Hermite polynomials, one for each coordinate variable. The data needed to define a p -th Hermite polynomial are the function value and all derivatives $\partial^{(\alpha_1 + \alpha_2 + \alpha_3)} / \partial \xi^{\alpha_1} \eta^{\alpha_2} \chi^{\alpha_3}$, $\max(\alpha_1, \alpha_2, \alpha_3) \leq p - 2$, at the eight corners of a cube in \mathbb{R}^3 . In our problem, the space over which the Hermite interpolation is defined is the $[-\ell_q/2, \ell_q/2]^3$ cube centered at $T(\vec{x}_q)$ in the (ξ, η, χ) coordinate system, and the data needed are \vec{x} and derivatives of T^{-1} at the vertices of this cube. Following the inverse function theorem, derivatives of T^{-1} can be computed by inverting the Jacobian matrix of T (or equivalent for higher derivatives). However, the location of these vertices are not known a priori in the (x, y, z) coordinate system. For this reason, instead of computing the needed data at the vertices, one can invert a linear system to fit a Hermite interpolation to data given at convenient locations. One particular choice are the vertices of the h_{Γ}^3 cube centered at \vec{x}_q and aligned with \hat{v}_1 , \hat{v}_2 , and \hat{v}_3 in the (x, y, z) coordinate system – see figure 5. We denote these vertices by $\vec{x}_{\vec{\gamma}}$, $\vec{\gamma} \in \{0, 1\}^3$.

Note that, since the interface is quasi-flat in a neighborhood of \vec{x}_q , the points $T(\vec{x}_{\vec{\gamma}})$ are close to the vertices of the cube in the (ξ, η, χ) coordinate system. Thus, the linear system that fits the Hermite interpolation through data given at $\vec{x}_{\vec{\gamma}}$ is close to the identity. The computation of T_{approx}^{-1} is summarized in algorithm 4. For ease of presentation, in algorithm 4 we

denote the Hermite interpolations collectively by $\vec{\mathcal{H}}$, and we use the notation $\vec{\theta} = \{\xi, \eta, \chi\}$ and $\vec{V} = \{\hat{v}_1, \hat{v}_2, \hat{v}_3\}$. Furthermore, step 4 of algorithm 4 represents the computation of derivatives of T^{-1} by application of the inverse function theorem.

Algorithm 4 Inverse transformation T_{approx}^{-1}

- 1: $\vec{x}_{\{0,0,0\}} \leftarrow \vec{x}_q - (h_\Gamma/2)\vec{v} \cdot \{1, 1, 1\}$
 - 2: $\vec{x}_{\vec{\gamma}} \leftarrow \vec{x}_{\{0,0,0\}} + (h_\Gamma)\vec{v} \cdot \vec{\gamma}, \quad \vec{\gamma} \in \{0, 1\}^3 \quad \triangleright \text{approximate corners}$
 - 3: $\vec{\theta}_{\vec{\gamma}} \leftarrow T(\vec{x}_{\vec{\gamma}})$
 - 4: $\left. \frac{\partial^{(\vec{\alpha})}\vec{x}}{\partial \vec{\theta}^{\vec{\alpha}}} \right|_{\vec{\theta}_{\vec{\gamma}}} \leftarrow \left(\left. \frac{\partial^{(\vec{\alpha})}\vec{\theta}}{\partial \vec{x}} \right|_{\vec{x}_{\vec{\gamma}}} \right)^{-1}, \max(\alpha_i) \leq p-2 \quad \triangleright \text{inverse function theorem}$
 - 5: Solve:

$$\begin{cases} \vec{\mathcal{H}}(\vec{\theta}_{\vec{\gamma}}) = \vec{x}_{\vec{\gamma}} \\ \frac{\partial \vec{\mathcal{H}}}{\partial \vec{\theta}}(\vec{\theta}_{\vec{\gamma}}) = \left. \frac{\partial^{(\vec{\alpha})}\vec{x}}{\partial \vec{\theta}^{\vec{\alpha}}} \right|_{\vec{\theta}_{\vec{\gamma}}} \end{cases}$$
-

The error introduced in approximating T^{-1} by a Hermite interpolation is $\mathcal{O}(h^{p+1}D^{(p+1)}T^{-1})$, where $D^{(p+1)}$ denotes derivatives of order $p+1$. Hence, an accurate approximation is only possible when derivatives of order $p+1$ are bounded. Furthermore, the derivatives of T^{-1} are related to the ratio ℓ_q/r_{\min} , *i.e.* to how flat the section of the interface is with respect to ℓ_q . We conjecture that, for a given p , it is possible to choose a constant $c > 0$ such that the condition $\ell_q/r_{\min} < c$ guarantees that $D^{(p+1)} = \mathcal{O}(1)$. For a spherical interface of constant curvature, and $p = 3$, we can show that $c \approx 0.4$. Thus we propose $\ell_q/r_{\min} < 0.4$ as a conservative upper bound that guarantees an accurate Hermite cubic approximation to T^{-1} in general circumstances.

Nevertheless, estimating r_{\min} in practice is not straightforward. For this reason, we prefer to use the determinant of the Jacobian on the $\xi - \chi$ plane,

$$\text{Jac} = \left\| \frac{\partial \vec{x}}{\partial \xi} \times \frac{\partial \vec{x}}{\partial \chi} \right\|_{T^{-1}(0, \xi, \chi)}, \quad (10)$$

evaluated at the Gaussian quadrature points as an indicator for the adequacy of the size of ℓ_q . As discussed in §3.3, the Jacobian is needed to compute the integrals over the interface. Hence, computing this indicator does not add to the computational cost of the present technique. For a spherical interface of

constant curvature, we can also show that $c = 0.4$ implies that $\text{Jac} > 0.83$. Hence, we use this threshold to verify whether ℓ_q is small enough in general cases.

3.3. Least squares statement

In §3.1 we show how to define a local coordinate transformation T that maps a quadrangular section of the interface into a square Q – see (8). One can impose the jump conditions on this section of the interface by computing integrals of the form

$$\int_{T^{-1}(Q)} \mathcal{F}^2 dS = \int_{-\ell_s/2}^{\ell_s/2} \int_{-\ell_s/2}^{\ell_s/2} \mathcal{F}^2(T^{-1}(0, \xi, \chi)) \left\| \frac{\partial \vec{x}}{\partial \xi} \times \frac{\partial \vec{x}}{\partial \chi} \right\|_{T^{-1}(0, \xi, \chi)} d\xi d\chi, \quad (11)$$

where \mathcal{F} represents a jump condition, such as (5b) or (5c). Furthermore, in §3.2 we introduce a scheme to evaluate the inverse transformation T^{-1} efficiently. Hence, one can evaluate (11) accurately and efficiently as

$$\int_{T^{-1}(Q)} \mathcal{F}^2 dS \approx \sum_i \left(w_i \mathcal{F}^2(T^{-1}(0, \xi_i, \chi_i)) \left\| \frac{\partial \vec{x}}{\partial \xi} \times \frac{\partial \vec{x}}{\partial \chi} \right\|_{T^{-1}(0, \xi_i, \chi_i)} \right) \quad (12)$$

where w_i corresponds to the weights of a numerical quadrature defined over $[-\ell/2, \ell/2]^2$, and (ξ_i, χ_i) are the integration points.

Nevertheless, our goal is to impose jump conditions on a piece of the interface that is approximately the size of the diagonal of the patch Ω_{Γ_i} . We achieve this goal by imposing the jump conditions over each individual quadrangular section individually, and adding the contributions of all sections whose union approximates the diagonal of the patch. Hence, we incorporate the new technique of imposing jump conditions in a least squares sense into the CFM by modifying the minimization function J_i to

$$\begin{aligned} J_i^{\text{new}} &= \frac{\ell_d^4}{V_i} \int_{\Omega_{\Gamma_i}} (\nabla^2 D - f_D)^2 dV \\ &\quad + \sum_{k=1}^{n_i} \frac{c_P}{S_{i_k}} \int_{\Gamma_{i_k}} [(D - a)^2 + \ell_d^2 (D_n - b)^2] dS, \end{aligned} \quad (13)$$

where Γ_i denotes the set of sections that approximate the diagonal of the patch. In practice, we add contributions from the of the n_i sections whose center are within a distance $\sqrt{2}\ell_d$ from the center of Ω_{Γ_i} .

4. Results

In this section we verify the accuracy and robustness of the new formulation of the CFM with examples in 2-D and 3-D. In the first two examples we reproduce 2-D problems discussed in ref. [1], and compare the accuracy of the new formulation to that of the an earlier implementation of the CFM. Furthermore, we also explore the concept of level set functions represented in independent grids and solve problems involving multiple interfaces close together.

The results we show here are computed with an overall fourth order accurate scheme. Namely, we discretize the Poisson equation using the standard 9-point stencil in 2-D, and the equivalent 19-point stencil in 3-D. Furthermore, we represent the correction function with Hermite cubic polynomials, which is consistent with fourth order of accuracy. Finally, we represent the interfaces using the Gradient-Augmented Level-Set(GALS) method [35], which is also based on Hermite cubic polynomials.

Below we use analytic expressions to define the model problems, but only the appropriate discrete data defined on a computational grid are inputted into the code. Here u denotes the solution, while ϕ denotes the level set function. We verify accuracy by evaluating the L_∞ norm of the error of the solution and its gradient.

4.1. Smooth 5-pointed star

Here we reproduce example 2 of ref. [1], which involves a smooth 5-pointed star. By considering a smooth interface we guarantee we can split the interface into quasi-flat segments, without the need of additional considerations around sharp corners. Furthermore, in this example G_P and G_Γ are the same grid. The problem is defined as follows.

- $\phi(x, y) = (x - 0.5)^2 + (y - 0.5)^2 - (0.25 + 0.05 \sin(5\varphi(x, y)))^2$.
- $\varphi(x, y) = \arctan\left(\frac{y - 0.5}{x - 0.5}\right)$.
- $\Omega_1 = \{(x, y) \in [0, 1]^2 \mid \phi(x, y) \leq 0\}$.
- $\Omega_2 = \{(x, y) \in [0, 1]^2 \mid \phi(x, y) > 0\}$.
- $u_1(x, y) = 0$.

- $u_2(x, y) = \exp(x) \cos(y)$.

Figure 6 shows the interface immersed into the Cartesian grid G_P used to solve the Poisson equation, along with a plot of the solution obtained with the CFM. Figure 7 shows a comparison of the error obtained with the new and earlier implementations of the CFM. In this figure we can observe that the new implementation converges to the expected fourth order of accuracy, albeit resulting in larger errors than the earlier implementation. We believe the larger errors are due to the use of the node-centered construction of the CFM patch. A different construction of the CFM patch is used in ref. [1]. As explained in ref. [1], this alternative patch construction results in smaller patches, which results in smaller errors. However, the node-centered approach seems to be more robust for general applications.

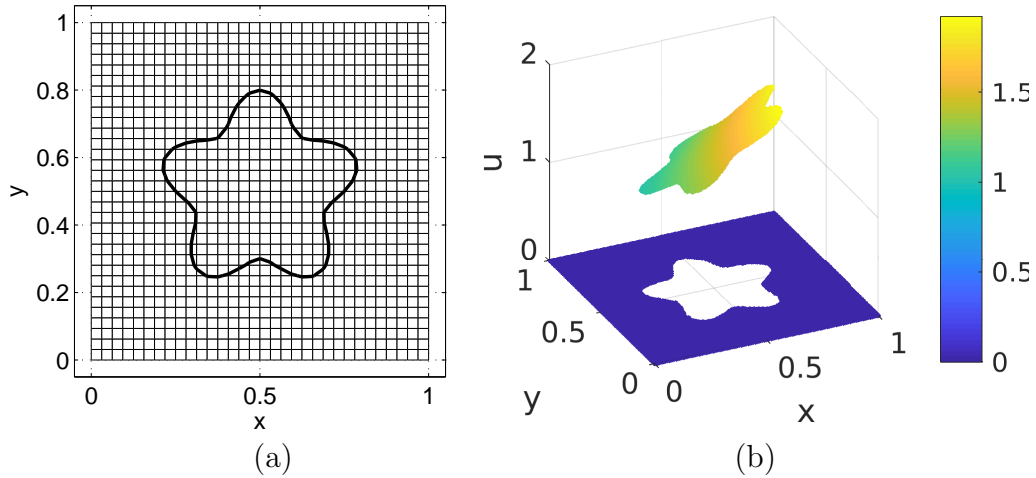


Figure 6: Example 1. (a) Interface immersed into G_P . (b) Solution obtained with the CFM.

4.2. Touching circles

We also reproduce example 5 of ref. [1], which involves two circular interfaces that touch at one point. In this example the interfaces are represented by level sets defined in independent grids: G_{Γ_1} and G_{Γ_2} . However, to be consistent with the implementation of ref. [1], we choose G_{Γ_1} and G_{Γ_2} to be the same as G_P . The problem is defined as follows.

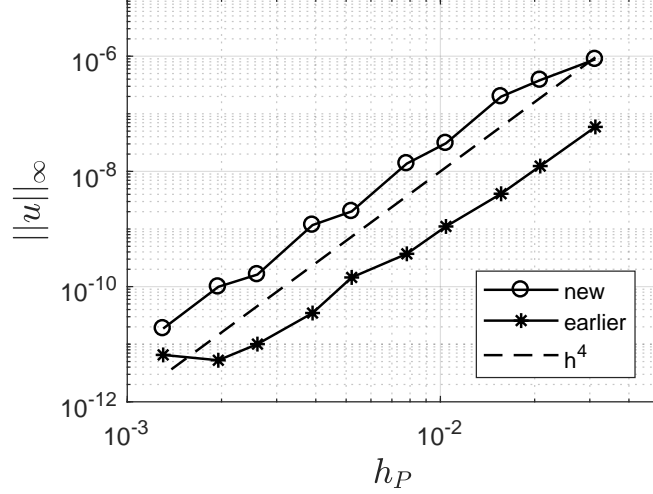


Figure 7: Example 1. Error convergence in the L_∞ norm. Comparison between new and earlier implementations of the CFM.

- $\phi_1(x, y) = (x - 0.5 - 0.2 \cos(\pi/e^2))^2 + (y - 0.5 - 0.2 \sin(\pi/e^2))^2 - 0.01$.
- $\phi_2(x, y) = (x - 0.5)^2 + (y - 0.5)^2 - 0.09$.
- $\Omega_1 = \{(x, y) \in [0, 1]^2 \mid \phi_1(x, y) \leq 0\}$.
- $\Omega_2 = \{(x, y) \in [0, 1]^2 \mid \phi_1(x, y) > 0, \phi_2(x, y) \leq 0\}$.
- $\Omega_3 = \{(x, y) \in [0, 1]^2 \mid \phi_1(x, y) > 0, \phi_2(x, y) > 0\}$.
- $u_1(x, y) = \sin(\pi x) \sin(\pi y) + 5$.
- $u_2(x, y) = \sin(\pi x) (\sin(\pi y) - \exp(\pi y))$.
- $u_3(x, y) = \exp(x) (x^2 \sin(y) + y^2)$.

Figure 8 shows the interfaces immersed into the Cartesian grid G_P used to solve the Poisson equation, along with a plot of the solution obtained with the CFM. Since the jump conditions (1b-c) are linear, one can solve for correction functions associated with each interface independently and combine them as needed – see remark 3. As shown in fig. 8(b), this approach allows for arbitrarily close interfaces

Remark 3. In practice, the interfaces seen by the CFM are subject to errors due to the level set representation. Hence, the “effective” interfaces are likely not to touch perfectly at just one point. They may cross over, or not touch at all. However, the CFM can handle these situations seamlessly by computing correction functions due to each of the interfaces independently. For instance, when the solution domain is subdivided into three regions by two interfaces, such as in figure ??, the CFM computes $D_{12} = u_2 - u_1$ and $D_{13} = u_3 - u_1$, where u_i denotes the solution restricted to each of the three regions. Since the jump conditions (1b-c) are linear, one can combine this information to compute $D_{23} = u_3 - u_2 = D_{13} - D_{12}$ as needed. ♣

Figure 9 shows a comparison of the error obtained with the new and earlier implementations of the CFM. Once again, the errors produced with the new implementation are larger than the ones produced with the earlier implementation, but the overall convergence is fourth order in both cases.

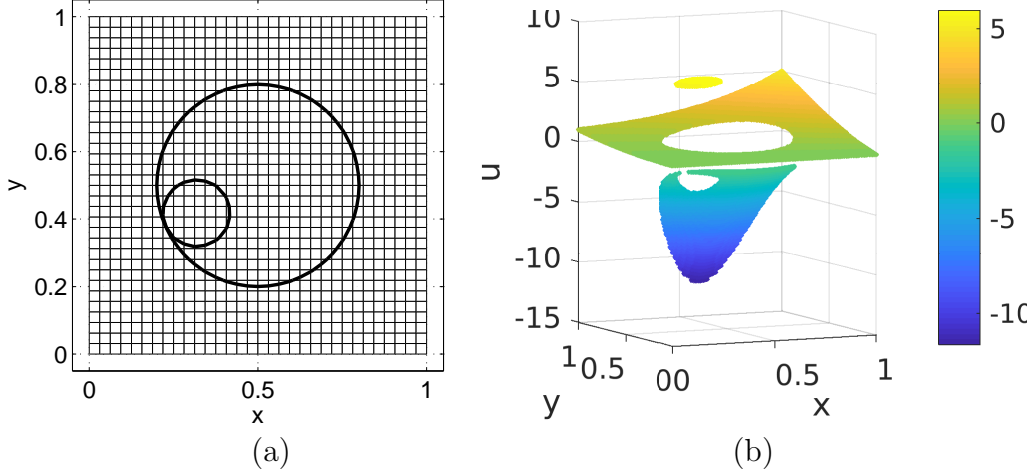


Figure 8: Example 2. (a) Interfaces immersed into G_P . Circles touch at single point. (b) Solution obtained with the CFM.

4.3. Three interfaces in 2-D

This 2-D example, not in [1], illustrates the application of the new implementation of the CFM to solve problems with more than two interfaces close together. Namely, we solve the following problem with three interfaces.

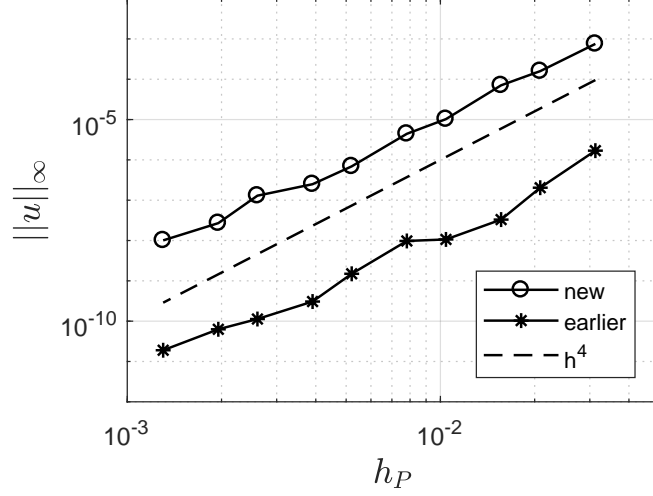


Figure 9: Example 2. Error convergence in the L_∞ norm. Comparison between new and earlier implementations of the CFM.

- $\phi_1(x_1, y_1) = (x_1 - 0.3)^2 + (y_1 - 0.3)^2 - 0.05$.
- $\phi_2(x_2, y_2) = (x_2 - 0.3)^2 + (y_2 - 0.3)^2 - (\sqrt{3}/10 + 0.05 \sin(5\varphi_2(x_2, y_2)))^2$.
- $\phi_2(x_3, y_2) = (x_3 - 0.25)^2 + (y_3 - 0.25)^2 - (0.15 + 0.05 \sin(2\varphi_3(x_3, y_3)))^2$.
- $\varphi_2(x_2, y_2) = \arctan\left(\frac{y_2 - 0.3}{x_2 - 0.3}\right)$.
- $\varphi_3(x_3, y_3) = \arctan\left(\frac{y_3 - 0.25}{x_3 - 0.25}\right)$.
- $\Omega_1 = \{(x_1, y_1) \in [0, 0.6]^2 \mid \phi_1(x_1, y_1) \leq 0\}$.
- $\Omega_2 = \{(x_2, y_2) \in [0, 0.6]^2 \mid \phi_2(x_2, y_2) \leq 0\}$.
- $\Omega_3 = \{(x_3, y_3) \in [0, 0.5]^2 \mid \phi_3(x_3, y_3) \leq 0\}$.
- $\Omega_4 = \{(x, y) \in [0, 1]^2 \mid \phi_i(x, y) > 0, i = 1, 2, 3\}$.
- $u_1(x, y) = \exp(x)(x^2 \sin(y) + y^2)$.
- $u_2(x, y) = \sin(\pi x) \sin(\pi y) + 10$.

- $u_3(x, y) = xy + 10$.
- $u_4(x, y) = 10(x^2 + y^2)$.

In this example the level set grids – G_{Γ_1} , G_{Γ_2} , and G_{Γ_3} – are not the same as G_P . In the expressions above, each level set is defined in terms of the Cartesian coordinates aligned with the corresponding grid. These coordinates are defined as follows.

$$\begin{aligned}
x_1 &= x - 0.34, \\
y_1 &= y - 0.37, \\
x_2 &= (x - 0.29) \cos(35\pi/180) + (y + 0.1) \sin(35\pi/180), \\
y_2 &= -(x - 0.29) \sin(35\pi/180) + (y + 0.1) \cos(35\pi/180), \\
x_3 &= (x - 0.885) \cos(75\pi/180) + (y + 0.048) \sin(75\pi/180), \\
y_3 &= -(x - 0.885) \sin(75\pi/180) + (y + 0.048) \cos(75\pi/180).
\end{aligned}$$

We illustrate the concept of independent level set grids in figure 10(a). In this figure we show G_{Γ_2} laid over G_P , along with the immersed interfaces. The solution obtained with the CFM is shown in figure 10(b). Once again we observe that the CFM produces good results in the presence of multiple interfaces. Furthermore, the error of the solution and its gradient² are plotted in figure 11. In addition to the expected fourth order convergence of the error in the solution, we also observe third order convergence of the error in its gradient.

²For clarity, we only show the error of u_x . The error of u_y behaves similarly.

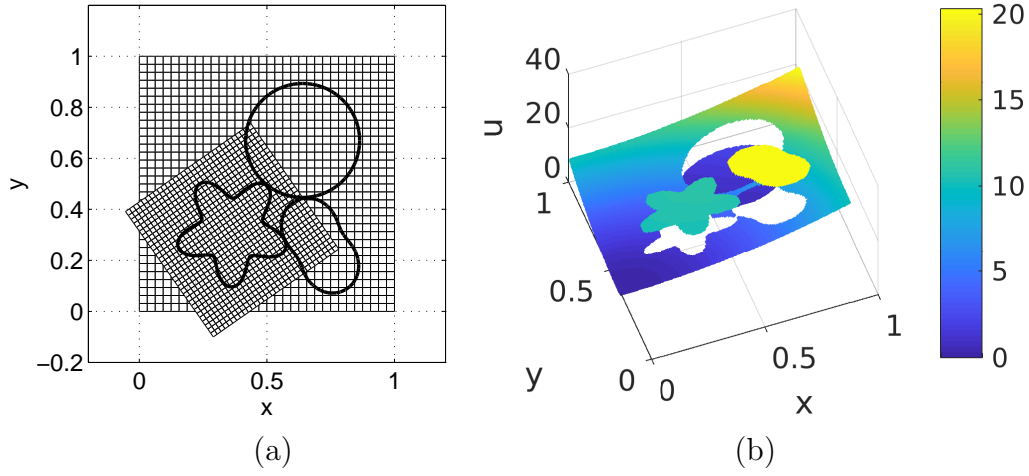


Figure 10: Example 3. (a) Interfaces immersed into G_P . The grid G_{Γ_2} used to represent ϕ_2 is also shown. (b) Solution obtained with the CFM.

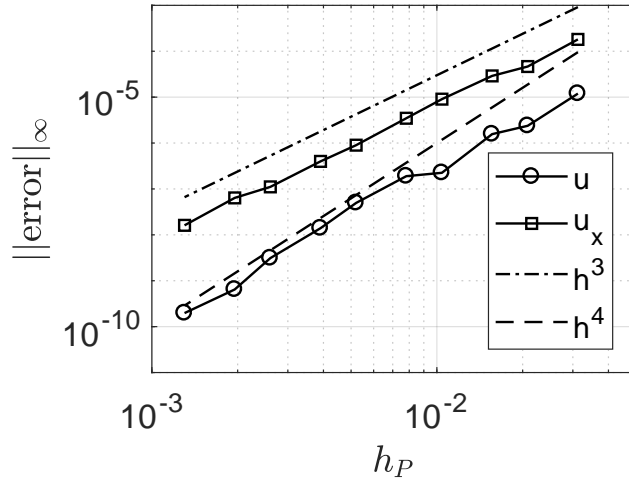


Figure 11: Example 3. Convergence of the error of in the solution and its x -derivative in the L_∞ norm.

4.4. Sphere with bumps

In this example we apply the new implementation of the CFM to solve the following 3-D problem, which is illustrated in figure 12.

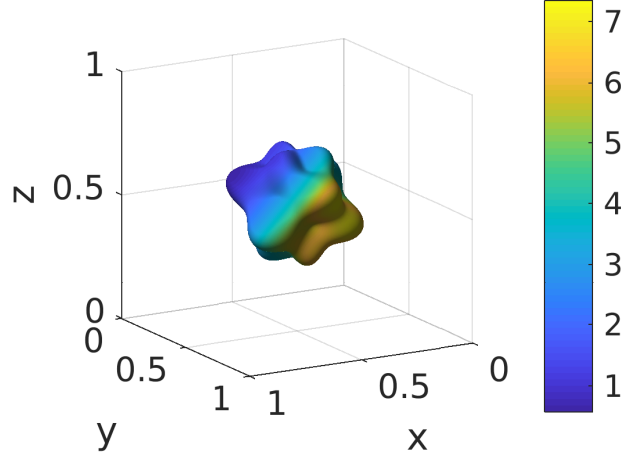


Figure 12: Example 4. Interface immersed into G_P , color-coded by the intensity of jump in the solution across it.

- $\phi(x_1, y_1, z_1) = (x_1 - 0.35)^2 + (y_1 - 0.35)^2 + (z_1 - 0.35)^2 - r^2$.
- $r(\varphi, \psi) = \sqrt{3}/8 + (0.28/\pi)(\varphi - \varphi^2/\pi) \sin(3\varphi) \sin(4\psi)$.
- $\varphi(x_1, y_1) = \arctan\left(\frac{y_1 - 0.35}{x_1 - 0.35}\right)$.
- $\psi(x_1, y_1, z_1) = \arccos\left(\frac{z_1 - 0.35}{\sqrt{(x_1 - 0.35)^2 + (y_1 - 0.35)^2 + (z_1 - 0.35)^2}}\right)$.
- $\Omega_1 = \{(x_1, y_1, z_1) \in [0, 0.7]^3 \mid \phi(x_1, y_1, z_1) \leq 0\}$.
- $\Omega_2 = \{(x, y, z) \in [0, 1]^3 \mid \phi(x, y, z) > 0\}$.
- $u_1(x, y, z) = \sin(\pi(x + z)/\sqrt{2}) \exp(\pi y)$.
- $u_2(x, y, z) = 0$.

In the expressions above, the level set ϕ is defined in terms of the Cartesian coordinates aligned with G_Γ . These coordinates are given by

$$\begin{aligned}x_1 &= x - 0.13, \\y_1 &= y - 0.1, \\z_1 &= z - 0.15.\end{aligned}$$

Figure 12 shows the interface, color-coded by the intensity in the jump in the solution across it. Figure 13 shows a 2-D slice of the solution computed with the CFM, as well as the interface immersed into the Cartesian grid at the slicing plane. The error of the solution and its gradient are plotted in figure 14³. We observe in this figure that also in 3-D the CFM results in fourth order of accuracy in the solution and third order of accuracy in its gradient.

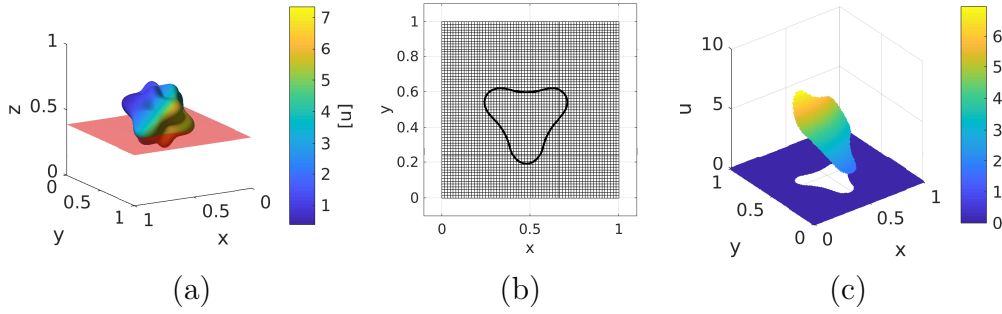


Figure 13: Example 4. 2-D slice of the solution. (a) Location of the slicing plane ($z = 0.39$). (b) The grid G_P . (c) Solution obtained with the CFM.

4.5. Touching spheres

This example is a 3-D extension of example 2 (§4.2). We consider two spherical interfaces that touch at a single point, as shown in figure 15. The interfaces are each represented using independent level set grids, and the problem is defined as follows.

- $\phi_1(x_1, y_1, z_1) = (x_1 - 0.4)^2 + (y_1 - 0.4)^2 + (z_1 - 0.4)^2 - 0.09$.

³For clarity, we only show the error of u_x . The errors of u_y and u_z behave similarly.

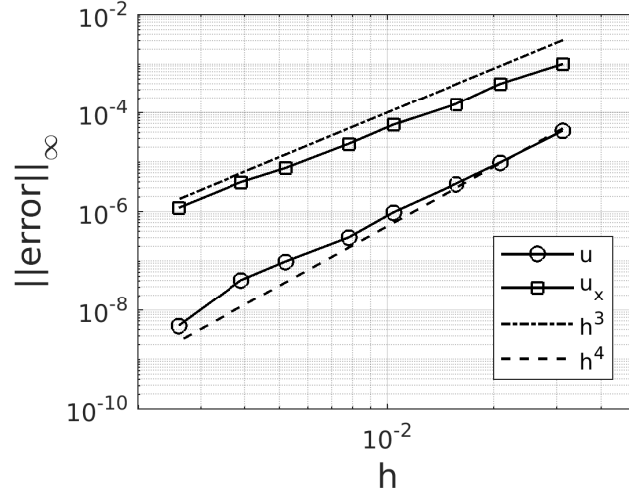


Figure 14: Example 4. Convergence of the error in the solution and its x -derivative in the L_∞ norm.

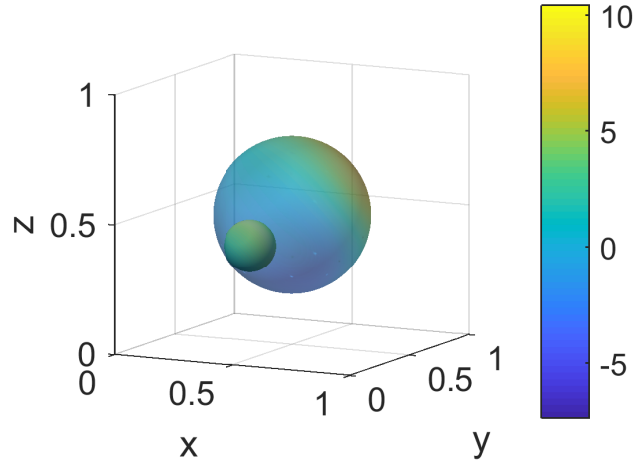


Figure 15: Example 5. Interfaces immersed into G_P , color-coded by the intensity of jump in the solution across it. Transparency is applied to the outer interface to show the internal interface. The spheres touch at a single point.

- $\phi_2(x_2, y_2, z_2) = (x_2 - 0.25)^2 + (y_2 - 0.25)^2 + (z_2 - 0.25)^2 - 0.01.$

- $\Omega_1 = \{(x_1, y_1, z_1) \in [0, 0.8]^3 \mid \phi_1(x_1, y_1, z_1) \leq 0\}$.
- $\Omega_2 = \{(x_2, y_2, z_2) \in [0, 0.5]^3 \mid \phi_2(x_2, y_2, z_2) \leq 0\}$.
- $\Omega_3 = \{(x, y, z) \in [0, 1]^3 \mid \phi_1(x, y, z) > 0, \phi_2(x, y, z) > 0\}$.
- $u_1(x, y, z) = (\sin(\pi x) \sin(\pi y) + 5) \log(x + z + 2)$.
- $u_2(x, y, z) = \sin(\pi(x + z))(\sin(\pi y) - \exp(\pi y))$.
- $u_3(x, y, z) = \exp(x)(x^2 \sin(y) + y^2) \cos(\pi z)$.

In the expressions above, the level sets are defined in terms of the respective grid coordinates, which are given by

$$\begin{aligned}
x_1 &= x - 0.1, \\
y_1 &= y - 0.1, \\
z_1 &= z - 0.1, \\
x_2 &= x - 0.25 - 0.2 \cos(\pi/e^2) \cos(\pi/3\varphi), \\
y_2 &= y - 0.25 - 0.2 \sin(\pi/e^2) \cos(\pi/3\varphi), \\
z_2 &= z - 0.25 - 0.2 \sin(\pi/3\varphi),
\end{aligned}$$

where φ denotes the golden constant,

$$\varphi = \frac{1 + \sqrt{5}}{2}.$$

Figure 15 shows the interfaces, color-coded by the intensity of the jump in the solution across them. Figure 16 shows a 2-D slice of the solution computed with the CFM on a plane close to the intersection point. The error of the solution and its gradient are plotted in figure 17⁴. Note that as in the 2-D examples, the accuracy of the solution and its gradient do not degrade even when interfaces are arbitrarily close.

⁴For clarity, we only show the error of u_x . The errors of u_y and u_z behave similarly.

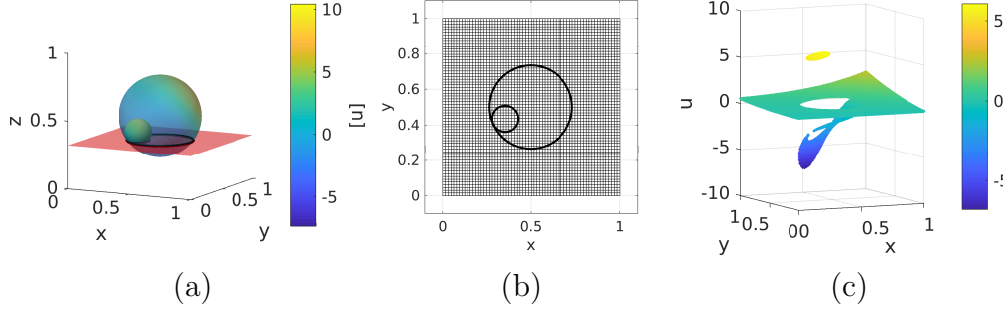


Figure 16: Example 5. 2-D slice of the solution. (a) Location of the slicing plane ($z = 0.39$). (b) The grid G_P . (c) Solution obtained with the CFM.

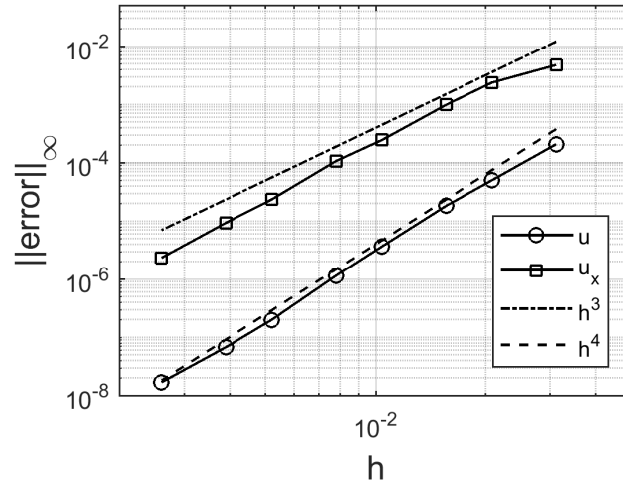


Figure 17: Example 5. Convergence of the error in the solution and its x -derivative in the L_∞ norm.

4.6. 3-D interfaces touching at two points

This final example shows the application of the CFM to a 3-D problem involving two interfaces that touch at two points, as shown in figure 18. The interfaces are each represented using independent level set grids, and the problem is defined as follows.

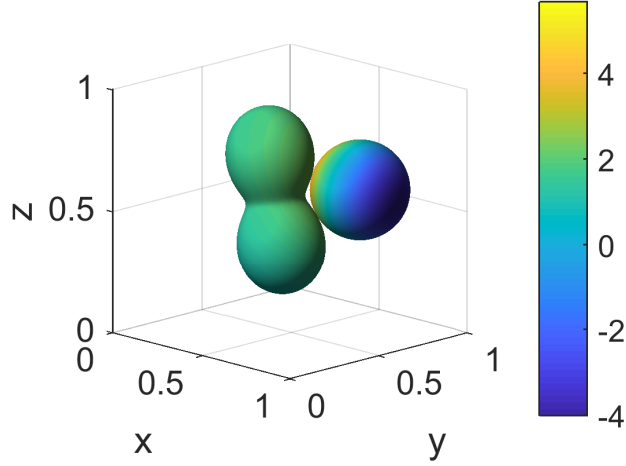


Figure 18: Example 6. Interfaces immersed into G_P , color-coded by the intensity of jump in the solution across it. The interfaces touch at two distinct points.

- $\phi_1(x_1, y_1, z_1) = (x_1 - 0.425)^2 + (y_1 - 0.425)^2 + (z_1 - 0.425)^2 - r^2$.
- $\phi_2(x_2, y_2, z_2) = (x_2 - 0.3)^2 + (y_2 - 0.3)^2 + (z_2 - 0.3)^2 - 0.04$.
- $r(\psi) = 0.25 + 0.13 \cos(2\psi)$.
- $\psi(x_1, y_1, z_1) = \arccos\left(\frac{z_1 - 0.425}{(x_1 - 0.425)^2 + (y_1 - 0.425)^2 + (z_1 - 0.425)^2}\right)$.
- $\Omega_1 = \{(x_1, y_1, z_1) \in [0, 0.85]^3 \mid \phi_1(x_1, y_1, z_1) \leq 0\}$.
- $\Omega_2 = \{(x_2, y_2, z_2) \in [0, 0.6]^3 \mid \phi_2(x_2, y_2, z_2) \leq 0\}$.
- $\Omega_3 = \{(x, y, z) \in [0, 1]^3 \mid \phi_1(x, y, z) > 0, \phi_2(x, y, z) > 0\}$.

- $u_1(x, y, z) = xyz$.
- $u_2(x, y, z) = \exp(x) \cos(y) \sin(z)$.
- $u_3(x, y, z) = \log(\sqrt{(x - 0.661)^2 + (y - 0.651)^2 + (z - 0.636)^2})$.

In the expressions above, the level sets are defined in terms of the respective grid coordinates, which are given by

$$\begin{aligned}
x_1 &= (x - 0.1) \cos(10\pi/180) + (z - 0.05) \sin(10\pi/180), \\
y_1 &= y - 0.05, \\
z_1 &= -(x - 0.1) \sin(10\pi/180) + (z - 0.05) \cos(10\pi/180), \\
x_2 &= x - 0.1047, \\
y_2 &= y - 0.1842, \\
z_2 &= z - 0.1249.
\end{aligned}$$

Figure 18 shows the interfaces, color-coded by the intensity of the jump in the solution across them. Figure 19 shows a 2-D slice of the solution computed with the CFM on a plane close to one of the touchings. The error in the solution and its gradient are plotted in figure 20. These results corroborate the accuracy of this implementation of the CFM, and its robustness with respect to interfaces that are arbitrarily close.

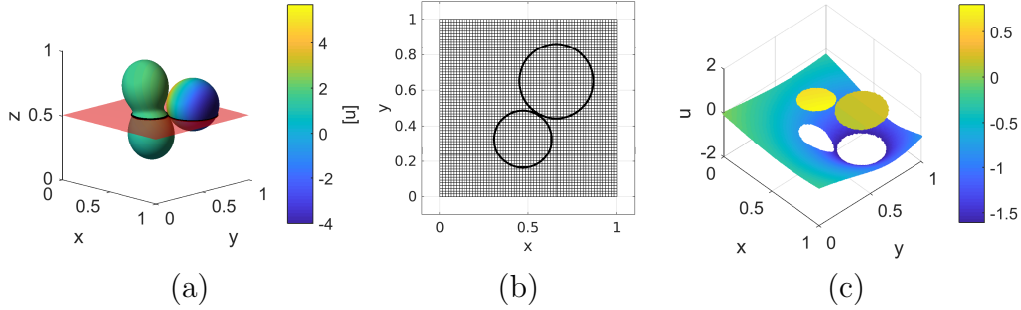


Figure 19: Example 6. 2-D slice of the solution. (a) Location of the slicing plane. (b) The grid G_P . (c) Solution obtained with the CFM.

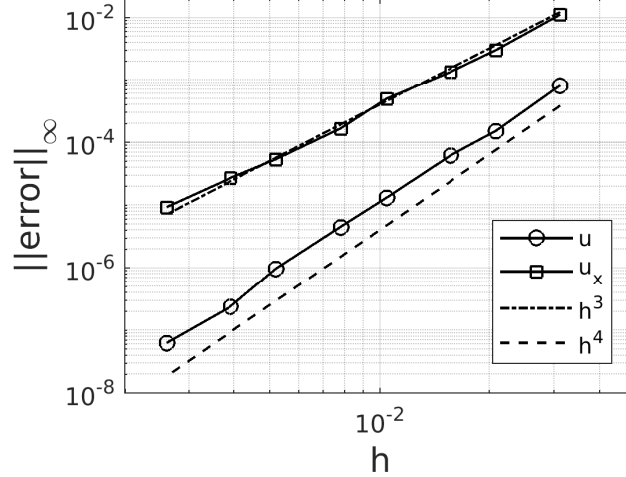


Figure 20: Example 6. Convergence of the error in the solution and its x -derivative in the L_∞ norm.

5. Conclusion

We present a new technique to impose jump conditions in a least squares sense. We also incorporate this technique into the *Correction Function Method* (CFM), resulting in a new formulation of the CFM that solves the Poisson equation when the solution is discontinuous across an interface that is represented implicitly (*e.g.*, as the zero contour of a level set function), both in 2-D and 3-D. Moreover, this new formulation of the CFM preserves the main features of the CFM, such as high order of accuracy and compact discretization stencils.

Imposing the jump conditions in a least squares sense is a key concept behind the CFM. However, this approach requires computing integrals over pieces of the interface, which is difficult when only an implicit representation of the interface is available, especially in 3-D. The new technique addresses this challenge by computing integrals only over sections of the interface that are amenable to numerical quadrature after appropriate coordinate transformations. In summary, the technique is based on the combination of (i) splitting the interface into small sections, (ii) defining local coordinate transformations that map these sections into squares, and (iii) an efficient scheme to compute of the transformations between local and global coordinates.

Our numerical experiments show that the formulation of the CFM that incorporates the new technique is efficient, accurate, and robust with respect to the arbitrary fashion the interface can intersect the computational grid. In particular, we show fourth order of accuracy when solving of the Poisson equation (1) when β is constant. An extension of this work to problems involving discontinuous β is the subject to a paper currently in preparation.

Acknowledgements

The authors would like to acknowledge the National Science Foundation support — this research was partially supported by NSF grants DMS-1719637 and DMS-1614043. In addition, the first author acknowledges the support by DARPA and AFOSR-COE. The second author also acknowledges support from the NSERC Discovery and Discovery Accelerator program.

References

References

- [1] A. N. Marques, J.-C. Nave, R. R. Rosales, A Correction Function Method for Poisson problems with interface jump conditions, *Journal of Computational Physics* 230 (20) (2011) 7567–7597. doi:10.1016/j.jcp.2011.06.014.
- [2] A. N. Marques, A Correction Function Method to solve incompressible fluid flows to high accuracy with immersed geometries, Ph.D. thesis, Massachusetts Institute of Technology (2012).
- [3] A. N. Marques, J.-C. Nave, R. R. Rosales, High order solution of Poisson problems with piecewise constant coefficients and interface jumps, *Journal of Computational Physics* 335 (2017) 497 – 515. doi:10.1016/j.jcp.2017.01.029.
- [4] C. S. Peskin, Flow patterns around heart valves: A numerical method, *Journal of Computational Physics* 10 (2) (1972) 252 – 271. doi:10.1016/0021-9991(72)90065-4.
- [5] C. S. Peskin, Numerical analysis of blood flow in the heart, *Journal of Computational Physics* 25 (3) (1977) 220–252. doi:10.1016/0021-9991(77)90100-0.

- [6] C. S. Peskin, B. F. Printz, Improved volume conservation in the computation of flows with immersed elastic boundaries, *Journal of Computational Physics* 105 (1) (1993) 33 – 46. doi:10.1006/jcph.1993.1051.
- [7] D. Goldstein, R. Handler, L. Sirovich, Modeling a no-slip flow boundary with an external force field, *Journal of Computational Physics* 105 (2) (1993) 354 – 366. doi:10.1006/jcph.1993.1081.
- [8] M.-C. Lai, C. S. Peskin, An immersed boundary method with formal second-order accuracy and reduced numerical viscosity, *Journal of Computational Physics* 160 (2) (2000) 705–719. doi:10.1006/jcph.2000.6483.
- [9] R. Cortez, M. Minion, The Blob Projection Method for immersed boundary problems, *Journal of Computational Physics* 161 (2) (2000) 428 – 453. doi:10.1006/jcph.2000.6502.
- [10] C. S. Peskin, The immersed boundary method, *Acta Numerica* 11 (2002) 479–517. doi:10.1017/S0962492902000077.
- [11] B. E. Griffith, C. S. Peskin, On the order of accuracy of the immersed boundary method: Higher order convergence rates for sufficiently smooth problems, *Journal of Computational Physics* 208 (1) (2005) 75–105. doi:10.1016/j.jcp.2005.02.011.
- [12] R. Mittal, G. Iaccarino, Immersed boundary methods, *Annual Review of Fluid Mechanics* 37 (1) (2005) 239–261. doi:10.1146/annurev.fluid.37.061903.175743.
- [13] D. B. Stein, R. D. Guy, B. Thomases, Immersed boundary smooth extension: A high-order method for solving PDE on arbitrary smooth domains using fourier spectral methods, *Journal of Computational Physics* 304 (2016) 252 – 274. doi:10.1016/j.jcp.2015.10.023.
- [14] H. Johansen, P. Colella, A Cartesian grid embedded boundary method for Poisson’s equation on irregular domains, *Journal of Computational Physics* 147 (1) (1998) 60–85. doi:10.1006/jcph.1998.5965.
- [15] A. Mayo, The fast solution of Poisson’s and the biharmonic equations on irregular regions, *SIAM Journal on Numerical Analysis* 21 (2) (1984) 285–299. doi:10.1137/0721021.

- [16] A. Mayo, The rapid evaluation of volume integrals of potential theory on general regions, *Journal of Computational Physics* 100 (2) (1992) 236–245. doi:10.1016/0021-9991(92)90231-M.
- [17] A. McKenney, L. Greengard, A. Mayo, A fast Poisson solver for complex geometries, *Journal of Computational Physics* 118 (2) (1995) 348 – 355. doi:10.1006/jcph.1995.1104.
- [18] R. J. LeVeque, Z. Li, The Immersed Interface Method for elliptic equations with discontinuous coefficients and singular sources, *SIAM Journal on Numerical Analysis* 31 (4) (1994) 1019–1044. doi:10.1137/0731054.
- [19] R. J. LeVeque, Z. Li, Immersed Interface Methods for Stokes flow with elastic boundaries or surface tension, *SIAM Journal on Scientific Computing* 18 (3) (1997) 709–735. doi:10.1137/S1064827595282532.
- [20] Z. Li, M.-C. Lai, The Immersed Interface Method for the Navier-Stokes equations with singular forces, *Journal of Computational Physics* 171 (2) (2001) 822–842. doi:10.1006/jcph.2001.6813.
- [21] L. Lee, R. J. LeVeque, An Immersed Interface Method for incompressible Navier-Stokes equations, *SIAM Journal on Scientific Computing* 25 (3) (2003) 832–856. doi:10.1137/S1064827502414060.
- [22] M. N. Linnick, H. F. Fasel, A high-order immersed interface method for simulating unsteady incompressible flows on irregular domains, *Journal of Computational Physics* 204 (1) (2005) 157 – 192. doi:10.1016/j.jcp.2004.09.017.
- [23] X. Zhong, A new high-order immersed interface method for solving elliptic equations with imbedded interface of discontinuity, *Journal of Computational Physics* 225 (1) (2007) 1066 – 1099. doi:10.1016/j.jcp.2007.01.017.
- [24] R. P. Fedkiw, T. Aslam, B. Merriman, S. Osher, A non-oscillatory Eulerian approach to interfaces in multimaterial flows (the Ghost Fluid Method), *Journal of Computational Physics* 152 (2) (1999) 457–492. doi:10.1006/jcph.1999.6236.

- [25] X.-D. Liu, R. P. Fedkiw, M. Kang, A boundary condition capturing method for Poisson's equation on irregular domains, *Journal of Computational Physics* 160 (1) (2000) 151–178. doi:10.1006/jcph.2000.6444.
- [26] M. Kang, R. P. Fedkiw, X.-D. Liu, A boundary condition capturing method for multiphase incompressible flow, *Journal of Scientific Computing* 15 (2000) 323–360. doi:10.1023/A:1011178417620.
- [27] F. Gibou, R. Fedkiw, A fourth order accurate discretization for the Laplace and heat equations on arbitrary domains, with applications to the Stefan problem, *Journal of Computational Physics* 202 (2) (2005) 577–601. doi:10.1016/j.jcp.2004.07.018.
- [28] F. Gibou, L. Chen, D. Nguyen, S. Banerjee, A level set based sharp interface method for the multiphase incompressible Navier-Stokes equations with phase change, *Journal of Computational Physics* 222 (2) (2007) 536–555. doi:10.1016/j.jcp.2006.07.035.
- [29] Y. C. Zhou, S. Zhao, M. Feig, G. W. Wei, High order matched interface and boundary method for elliptic equations with discontinuous coefficients and singular sources, *Journal of Computational Physics* 213 (1) (2006) 1 – 30. doi:10.1016/j.jcp.2005.07.022.
- [30] A. Guittet, M. Lepilliez, S. Tanguy, F. Gibou, Solving elliptic problems with discontinuities on irregular domains – the Voronoi Interface Method, *Journal of Computational Physics* 298 (2015) 747–765. doi:10.1016/j.jcp.2015.06.026.
- [31] Z. Li, T. Lin, X. Wu, New Cartesian grid methods for interface problems using the finite element formulation, *Numerische Mathematik* 96 (2003) 61–98. doi:10.1007/s00211-003-0473-x.
- [32] S. Hou, X.-D. Liu, A numerical method for solving variable coefficient elliptic equation with interfaces, *Journal of Computational Physics* 202 (2) (2005) 411–445. doi:10.1016/j.jcp.2004.07.016.
- [33] S. Hou, P. Song, L. Wang, H. Zhao, A weak formulation for solving elliptic interface problems without body fitted grid, *Journal of Computational Physics* 249 (0) (2013) 80 – 95. doi:10.1016/j.jcp.2013.04.025.

- [34] D. S. Abraham, A. N. Marques, J.-C. Nave, A Correction Function Method for the Wave Equation with Interface Jump Conditions, ArXiv e-prints [arXiv:1609.05379](#).
- [35] J.-C. Nave, R. R. Rosales, B. Seibold, A gradient-augmented level set method with an optimally local, coherent advection scheme, *Journal of Computational Physics* 229 (10) (2010) 3802–3827. doi:[10.1016/j.jcp.2010.01.029](#).